ELSEVIER

Contents lists available at ScienceDirect

Automation in Construction

journal homepage: www.elsevier.com/locate/autcon





Monitoring of pipelines subjected to interactive bending and dent using distributed fiber optic sensors

Xiao Tan^a, Sina Poorghasem^a, Ying Huang^b, Xin Feng^c, Yi Bao^{a,*}

- a Department of Civil, Environmental and Ocean Engineering, Stevens Institute of Technology, Hoboken, NJ 07030, United States
- b Department of Civil, Construction, and Environmental Engineering, North Dokota State University, Fargo, ND 58102, United States
- ^c Faculty of Infrastructure Engineering, Dalian University of Technology, Dalian, Liaoning 116024, China

ARTICLE INFO

Keywords: Condition monitoring Distributed fiber optic sensors (DFOS) Interactive anomalies Optical frequency domain reflectometry (OFDR) Pipeline safety

ABSTRACT

Interactive anomalies of pipelines represent important contributors to pipeline incidents, but monitoring interactive anomalies is challenging. This paper presents an approach to monitor interactive bending and dent deformations that occur at the same pipeline section. The proposed approach utilizes distributed fiber optic sensors to measure strain distributions of pipelines with a high resolution (0.65 mm) in real time. Steel pipes instrumented with fiber optic cables along their length and circumference directions were tested under four-point bending to generate interactive bending and dent deformations. The strain distributions measured from the distributed sensors were analyzed to detect, locate, quantify, visualize, and distinguish interactive bending and dent deformations in the loading process. The strains measured from distributed fiber optic sensors aligned with those measured from fiber Bragg grating sensors, displacement sensors, and computer vision. This study enhances the ability to monitor interactive threats in pipelines, contributing to improved condition assessments and infrastructure resilience.

1. Introduction

Pipelines offer a highly dependable method for transporting energy products such as oil and gas, especially in challenging conditions such as deep water and underground [1]. Despite the benefits of pipelines, the potential threats to pipeline integrity, arising from various anomalies, become more pronounced with the expansion of pipeline networks. There is a compelling need for extensive research and development to enhance the capabilities of detecting and assessing the anomalies of pipelines at an early stage.

In literature, numerous sensing technologies have been developed for monitoring individual anomalies of pipelines such as electrochemical methods for corrosion [2], caliper methods for dents [3], and electrical strain gauges for cracks [4]. However, there is a scarcity of methods that can detect multiple types of anomalies that coincide in a pipeline section simultaneously. Those anomalies that occur at the same position of a pipeline are called interactive anomalies, which can result in a higher likelihood of failure than individual anomalies. For instance, pipelines are susceptible to ground motions such as faults and landslides, which tend to cause bending failures. Meanwhile, third-party construction and excavation activities can exert pressure on pipelines, causing permanent

plastic dents locally. The dents may appear in sections subjected to bending, thereby leading to combined bending and dents at the same position of a pipe. According to the Pipeline and Hazardous Materials Safety Administration (PHMSA) of United States Department of Transportation, combined threats have caused large risks to pipeline safety than individual threats because different threats often promote each other [5]. Research showed that dents posed greater risks when they occur on the compression side of a pipeline [6]. This is because of the significant curvature alteration of the pipe wall within the deformed region, resulting in an abrupt change in angle. Consequently, it is important to monitor bending and dents in the same position.

To detect interactive anomalies, computer vision methods have been developed, capable of identifying and quantifying various types of damage, such as cracks [7], corrosion [8], and dents [9]. The vision-based techniques employ non-contact sensors, such as cameras [10], laser scanners [11], and other digital imaging devices [12]. However, it is important to note that vision-based methods are limited to surface measurements and susceptible to various environmental factors such as precipitation and lighting conditions, which may affect their performance significantly.

In addition to vision-based methods, various sensing technologies

^{*} Corresponding author.

E-mail address: yi.bao@stevens.edu (Y. Bao).

have been developed for inspecting pipelines. One of the popular methods is to use in-line inspection (ILI) technologies by employing pipeline inspection gauges (PIGs), which are robots equipped with non-destructive testing (NDT) devices such as calipers and magnetic flux leakage devices [3,13,14]. As PIGs pass through pipelines, their sensing devices are used to detect pipeline anomalies, providing valuable information for assessing pipeline conditions [15,16]. However, there are "unpiggable" pipelines that cannot be inspected using PIGs, and it is difficult to analyze data from various sensing devices [17,18]. In addition, ILI is typically performed periodically with substantial time intervals that poses challenges for timely identification of pipeline anomalies [19].

To enable timely detection of anomalies, in-situ sensors have attracted increasing interests. For example, fiber optic sensors have been applied for real-time monitoring of pipelines because of their various advantages such as high precision, physical and chemical stability, durability, immunity to electromagnetic interference, and small size [20–22]. Fiber optic sensors can be categorized into point sensors, such as grating-based sensors and interferometer-based sensors, and distributed sensors which utilize a single fiber optic cable to continuously monitor the entire pipeline length and provide thousands of sensing points [23].

Based on literature review, distributed fiber optic sensors (DFOS) have been applied to monitor different types of individual anomalies of pipelines, such as crack, leakage, dent, corrosion, and so on [24-38]. Distributed temperature and strain sensors were strategically deployed along pipes to measure temperature and strain distributions [24,33,36-38]. These measurements were utilized to evaluate the condition of pipelines. For example, Lalam et al. used distributed fiber optic sensors for flow monitoring [36]. Li et al. used distributed fiber optic sensors to monitor pipeline leakage and pipe-soil interaction [37,38]. Fiber optic sensors were also employed to detect and quantify pipeline corrosion through monitoring corrosion-induced dimensional changes [25,26,32,34]. Alternative methods for assessing pipeline corrosion involve the measurement of chemical substances or humidity levels associated with the corrosion process [29,35]. Furthermore, a comprehensive literature review of DFOS utilized for monitoring pipeline deformation subjected to strain transfer effect was provided in reference [30]. Brillouin scattering-based distributed fiber optic sensing technologies, such as Brillouin optical time domain analysis and Brillouin optical time domain reflectometry, are available for long-haul operations (> 100 km) [27,28].

Currently, there is lack of research on applying DFOS to monitor interactive anomalies, which often occur in realistic pipeline structures. Specifically, two main challenges have been identified from literature: (1) It remains unknown whether DFOS can be applied and how they can be applied for interactive anomalies. The main challenges of monitoring interactive anomalies using DFOS are associated with the complexity of strain fields that are dependent on different anomalies. (2) Research on strain-based evaluation methods of interactive anomalies severity is rare [39]. There is an urgent need for developing practical and effective methods to quantitatively discriminate anomalies using DFOS data. In a nutshell, it is still unclear how to monitor interactive anomalies based on DFOS. Specifically, when a DFOS is utilized to measure interactive bending and dent on pipelines, the following questions still need to be answered: (1) How do dents affect the strain distribution in fiber optic cables installed on a pipe subjected to bending deformations? (2) When will interactive bending and dent be initiated on pipelines? (3) How to evaluate and discriminate bending and dent based on DFOS data? These knowledge gaps have stalled wider applications of DFOS because it is unknown how to properly interpret the distributed strain sensing data in the presence of interactive bending and dent deformations.

To address these challenges, the overarching goal of this study is to develop an approach for assessing and discriminating global and local deformations of pipelines using DFOS. The main research objectives are threefold: (1) To investigate the performance of DFOS for monitoring

bending and dents occurring at the same position of a pipe. (2) To develop a method to assess pipeline condition using DFOS, including the processing and interpretation of sensor data for condition assessment. (3) To develop an interactive deformation model to quantitatively evaluate interactive dent and bending effects under different loads by using normalized power spectra.

To achieve the above objectives, in this research, laboratory tests were conducted using pipe specimens instrumented with DFOS. The pipe specimens were subjected to four-point bending to investigate interactive bending and dent effects. Strain distributions were measured from the DFOS and utilized to detect, locate, quantify, visualize, and separate interactive threats of bending and dent deformations.

This research has two main novelties: (1) A new strain-based dent severity evaluation method is developed to monitor the dents of pipelines subjected to bending deformations. The method is different from the current practices that use dent depth-based criterion for dent assessment, which may lead to an inaccurate conclusion [40]. (2) A model is developed to discriminate interactive effects between bending and dent based on DFOS data. This research supports the early detection of interactive anomalies and helps improve the maintenance and management of pipelines.

The remainder of the paper is structured as follows: Section 2 introduces the fiber optic cables, the sensing principle, and the proposed methods; Section 3 presents the laboratory experimental program conducted using large pipes; Section 4 analyzes and discusses the experimental results; and Section 5 summarizes the new findings obtained from this study.

2. Methods

2.1. Research framework

Fig. 1 shows the framework of this research. Distributed fiber optic sensors are deployed on the surface of pipelines to measure strain distributions along the length of the distributed fiber optic sensors.

The measured strains are used to determine the strain distributions and deformed profiles of pipes. Then, the strain distributions are utilized to evaluate the dent severity of pipes. Finally, an interactive deformation model is developed to quantitatively evaluate interactive dent and bending effects using normalized power spectra. It is envisioned that the interactive deformation model is applicable to support early detection of interactive anomalies. More details about the distributed fiber optic sensing, interactive deformation model, and calculation of deformations are elaborated in Sections 2.2 to 2.4, respectively.

2.2. Distributed fiber optic sensing

2.2.1. Fiber optic cables

Two types of telecommunication-grade single-mode fiber optic cables (supplier: Fiber Instrument Sales) were used as DFOS (Fig. 2). These fiber optic cables served as both distributed sensors and transmission lines. The fiber optic cable used for strain measurement comprised a glass core (diameter: 8.2 µm), a glass cladding (outer diameter: 125 µm), an inner coating (outer diameter: 190 μ m), and an outer coating (outer diameter: 242 µm). The core and cladding are the sensing parts. Light waves are propagated along the cable through total internal reflection at the core-cladding interface. The inner coating consisted of a soft acrylic layer to ensure durability and protection from mechanical impact, and the outer coating consisted of a stiff acrylic layer to protect the glass fiber from abrasion and environmental exposure. The elastic moduli of the glass fiber, inner coating, and outer coating were 72 GPa, 0.6 MPa, and 2 MPa, respectively. A polyvinyl chloride (PVC) tight buffer layer with a diameter of 900 μm was applied to further enhance the mechanical strength and facilitate the operation of the fiber in practice.

The fiber optic cable for temperature compensation consisted of a fiber optic strain cable, a layer of aramid yarn, and a cable jacket. The

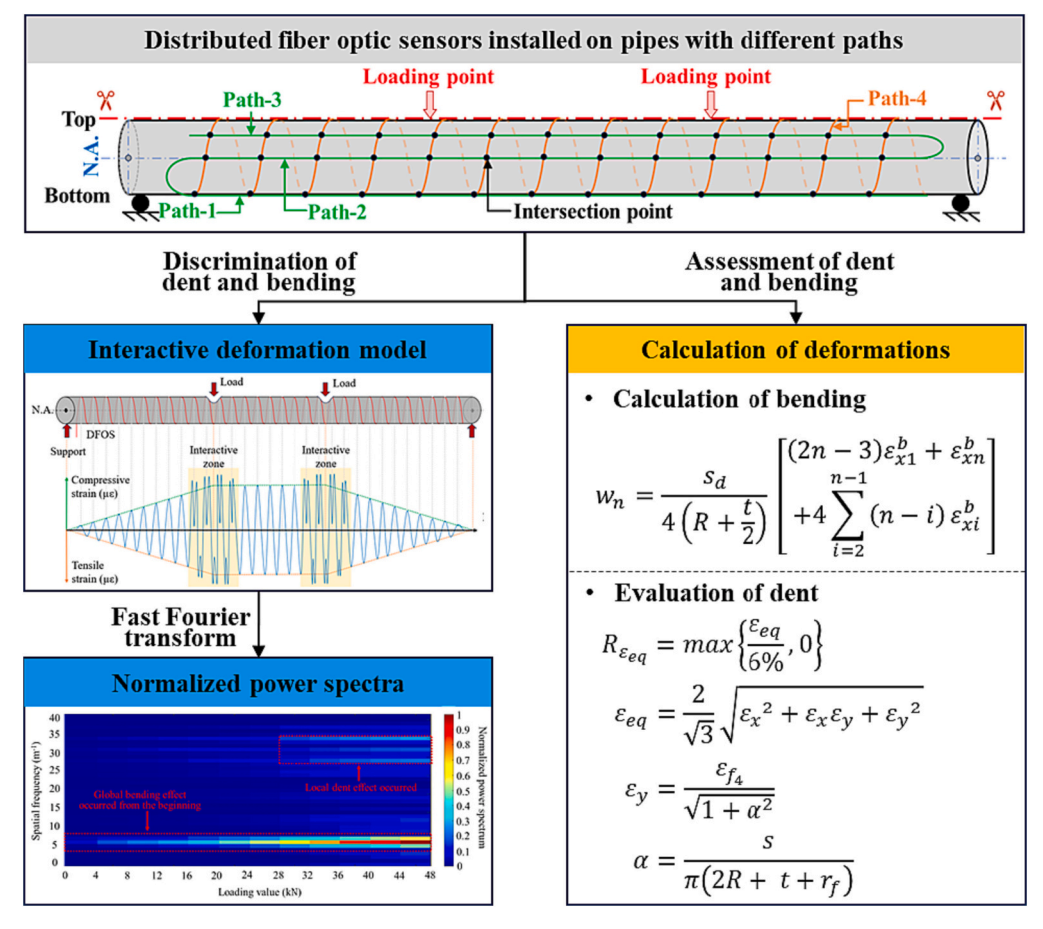


Fig. 1. Framework for assessing and discriminating interactive dent and bending in pipelines.

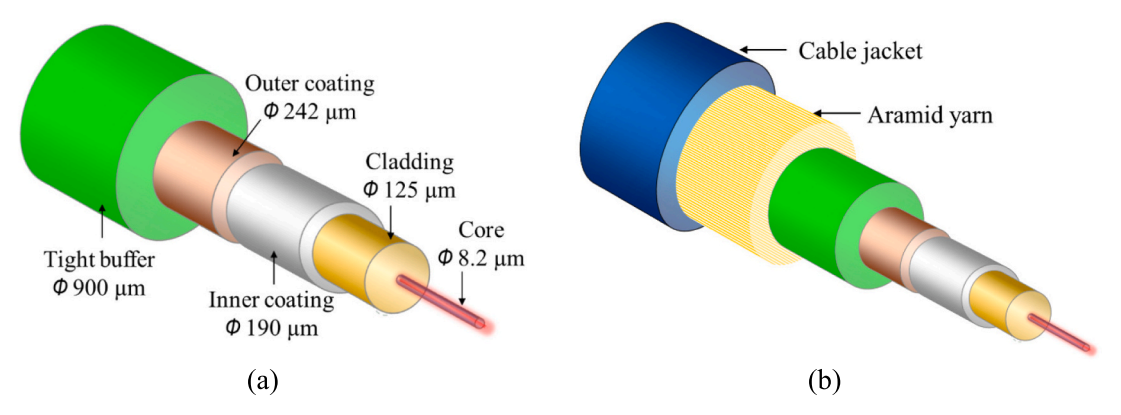


Fig. 2. Cross sections of the fiber optic cables for measuring: (a) strain, and (b) temperature.

aramid yarn made from Kevlar® is crimped to the cable jacket. Therefore, forces applied to the cable are taken by the aramid yarn instead of the fiber. Thus, the fiber optic cable is free of mechanical strains and only sensitive to temperature. Finally, a jacket is applied outside the yarn and fiber further mechanical protection. The jacket is typically made of a soft plastic material with a thickness of about 1 mm.

2.2.2. Sensing principle

Rayleigh scattering is a phenomenon in fiber optic cables where transmitted light undergoes elastic scattering due to the irregular microstructure of the fiber. One example of such irregular microstructure is the variation in glass composition, leading to changes in the refractive index and density of the fiber. This research adopted the

Optical Frequency Domain Reflectometry (OFDR) technology to measure strain and temperature based on Rayleigh scattering at reference and perturbed states. In each state, a light wave is launched into the fiber optic cable, resulting in Rayleigh backscattering. The backscattered signal is collected along the fiber length. At each point of the fiber, the amplitude of the backscattered signal is plotted against the wavelength of the light. Fast Fourier Transform (FFT) is applied to obtain intensity versus frequency data. A cross-correlation operation is then conducted between the reference and perturbed states, identifying a frequency shift for each location along the optical fiber. The frequency shift is associated with the strain and temperature changes of the fiber core. The distance is determined by calculating the traveling time of the backscattered light wave [35].

In this study, a data acquisition system (model: Luna ODISi 6102) was adopted to conduct OFDR measurement. The manufacturer-specified accuracies for strain and temperature are 5 $\mu\epsilon$ and 0.9 °C, respectively [40]. The maximum sensing length of the system is >200 m in each channel, and the system has eight independent channels [40]. More details about the sensing principle and prior applications of OFDR are available in references [41, 42]. The frequency shift observed in the measurements is associated with changes in strain and temperature:

$$\frac{\Delta \lambda}{\lambda} = \frac{\Delta v}{v} = K_T T + K_e \varepsilon \tag{1}$$

where λ and v refer to the mean optical wavelength and frequency, respectively; K_T and K_ε refer to the temperature (T) and strain (ε) calibration constants, respectively. The values of K_T and K_ε were experimentally calibrated as elaborated in our previous studies [25,41].

In this study, an OFDR system and laboratory experiments were used to develop and evaluate the proposed approach. In real practices, it is often unnecessary to monitor the entire pipe length since interactive threats usually exist in certain risky regions such as the regions with severe ground motions. The proposed technology and OFDR system can be applied to monitor critical segments of the pipeline network. In real practices, if the length of the pipeline segment that needs to be monitored is longer than the maximum sensing distance of a single channel of an OFDR system, multiple distributed sensors can be used for different portions of the segment. When the data acquisition system has multiple channels, it can be placed in the middle of two adjacent segments to double the measurement distance by using two channels for both sides of the pipe length. An alternative solution of extending the sensing distance is to use Brillouin scattering-based systems which can achieve sensing lengths longer than 100 km. A tradeoff for the longer sensing distance is the lower spatial resolution. For example, a pulse-pre-pump BOTDA (PPP-BOTDA) system had a sensing length longer than 1 km while the spatial resolution was up to 20 mm [43-46].

2.3. Interactive deformation model

strain (με)

The proposed sensor deployment pattern is shown in Fig. 3. A pair of DFOS that include a distributed strain sensor and a distributed temperature sensor are deployed on the surface of a pipe in a helix pattern. The distributed temperature sensor is used for temperature

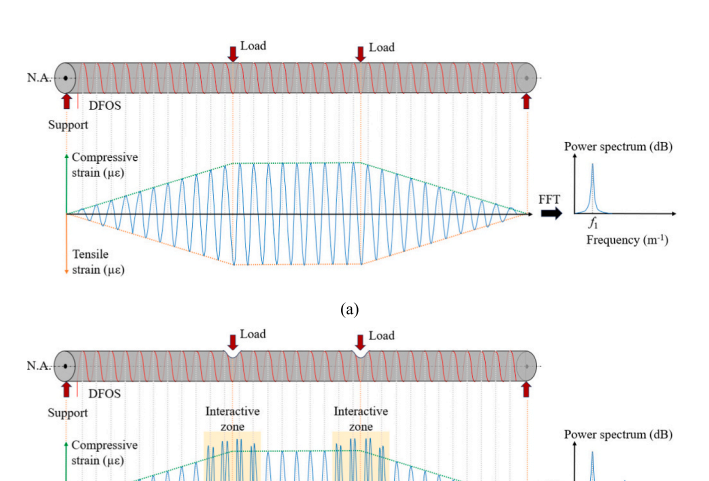


Fig. 3. Conceptual illustration of strain distributions measured from a pipe subjected to bending: (a) before the generation of dent; and (b) after the generation of dent. "N.A." denotes neutral axis.

(b)

compensation. When the pipe is subjected to bending, the distributed strain sensor measures strains, showing periodic changes along the pipe length, as shown in Fig. 3(a). These periodic changes of strain distribution are consistent with the experimental results from previous research [39].

The periodic changes are attributed to the deployment of DFOS, which pass through the compressive and tensile zones of the pipe back and forth. As the load increases, the magnitudes of the strains increase while the periodic pattern retains. To characterize the periodic feature of a strain distribution, FFT can be performed to convert the strain distribution from a spatial domain to a frequency domain. The characteristic frequency is denoted by f_1 , which is determined by the deployment (i.e., the spacing between adjacent loops) of DFOS.

With the further increase of the applied load, local dents will be generated at the loaded spots, as shown in Fig. 3(b). The presence of dent deformations will influence the strain distributions and introduce high-frequency components to the periodic changes of strain distributions. The characteristic frequency of dent deformations is denoted by f_2 , which is associated with the deployment pattern of DFOS as well as the dent deformations.

This paper proposes to detect the presence and development of dents based on the measured strain distributions from DFOS deployed on pipelines. The appearance of new high-frequency components (f_2) is used to judge the appearance of dents in a pipe. The positions of interactive zones are utilized to determine the positions of dents in the pipe. The severity of dents will be assessed by the magnitude of the strains, which are elaborated in the next section.

2.4. Calculation of deformations

A general description of the strains at a dent spot of a pipe is shown in Fig. 4. The strain is composed of a longitudinal strain (ε_x) and a circumferential strain (ε_y) . Each of these strains can be further divided into a bending strain (ε^b) and a membrane strain (ε^m) . The membrane strain is even along the wall thickness, whereas the bending strains exhibit linear changes from the inner to the outer surface of the pipe wall.

The governing equations that describe the relationship between the strain and the out-of-plane deformation are shown as follows [47]:

$$\varepsilon_x^b = (R+h)\frac{\partial^2 w}{\partial x^2}$$
 (2a)

$$\varepsilon_{y}^{b} = h \frac{\partial^{2} w}{\partial v^{2}} \tag{2b}$$

$$\varepsilon_x^m = \frac{\partial u}{\partial x} + \frac{1}{2} \left(\frac{\partial w}{\partial x} \right)^2 \tag{2c}$$

$$\varepsilon_y^m = \frac{\partial v}{\partial x} - \frac{w}{z} + \frac{1}{2} \left(\frac{\partial w}{\partial y} \right)^2 \tag{2d}$$

where u, v, and w are the displacements along the longitudinal (x), circumferential (y), and radius (z) directions, respectively; ε_x^b and ε_y^b are the longitudinal and circumferential bending strains, respectively; ε_x^m and ε_y^m are the longitudinal and circumferential membrane strains, respectively; h is the distance from the mid-surface (neutral plane) of pipe wall; t is pipe wall thickness; and R is the mean radius of the pipe.

If the pipe is only subjected to bending and dent, the membrane strain (ε_x^m) can be neglected [47,48]. Since the direction of dent is negative along radius z and the maximum bending strain occurs at the external surface (i.e., h=t/2), eq. (1) can be rewritten into a simplified form:

Frequency (m⁻¹)

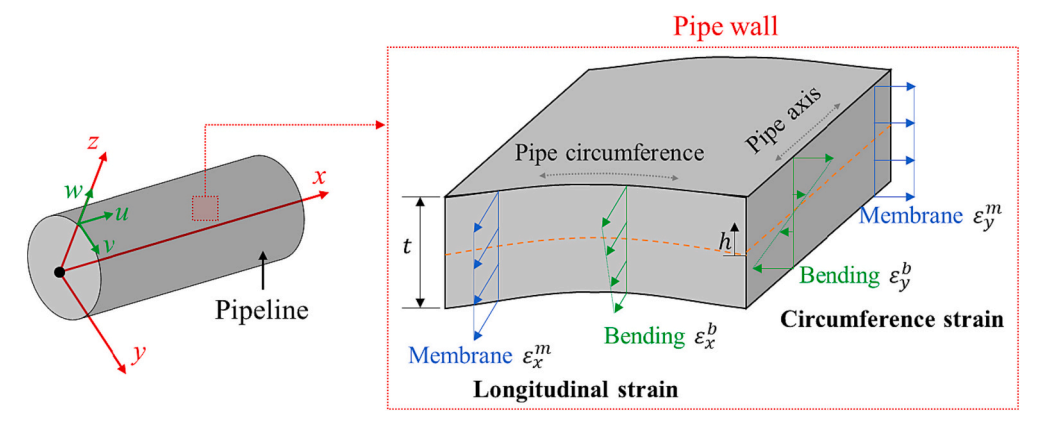


Fig. 4. Distribution of the different strain components of a pipe with a constant wall thickness.

$$\varepsilon_x = \varepsilon_x^b = \left(R + \frac{t}{2}\right) \frac{\partial^2 w}{\partial x^2} \tag{3a}$$

$$\varepsilon_{y} = \varepsilon_{y}^{b} + \varepsilon_{y}^{m} = \frac{t}{2} \frac{\partial^{2} w}{\partial y^{2}} + \frac{\partial v}{\partial x} - \frac{w}{R + \frac{t}{2}} + \frac{1}{2} \left(\frac{\partial w}{\partial y}\right)^{2}$$
(3b)

If the longitudinal strain profile along the pipe is measured, the bending deformation of the pipe can be calculated by integrating the differential eq. (3a):

$$w(x) = \int_{0}^{x} \int_{0}^{x} \frac{\varepsilon_x^b}{R + \frac{t}{2}} dx dx + Ax + B$$
 (4)

where *A* and *B* are the constants determined by boundary conditions. According to trapezoidal integration, eq. (4) can be re-written as:

$$w_n = \frac{s_d}{4(R + \frac{t}{2})} \left[(2n - 3)\varepsilon_{x1}^b + \varepsilon_{xn}^b + 4\sum_{i=2}^{n-1} (n - i)\varepsilon_{xi}^b \right]$$
 (5)

where w_n is the displacement of the n-th point; and s_d is the distance between measuring points.

The membrane and bending strains can be combined into an equivalent strain (ε_{eq}) on the exterior surface of a pipe, as shown in eq. (6), and ε_{eq} can be utilized to evaluate dent severity [47–49]. In engineering practices, appropriate empirical criteria can be adopted based on ε_{eq} . For example, a dented pipe is safe when the maximum ε_{eq} is smaller than 6% in reference [45].

$$\varepsilon_{eq} = \frac{2}{\sqrt{3}} \sqrt{\varepsilon_x^2 + \varepsilon_x \varepsilon_y + \varepsilon_y^2}$$
 (6)

Based on the equivalent strain, an indicator is defined to characterize the severity of dent, as shown in eq. (7):

$$R_{\varepsilon_{eq}} = max \left\{ \frac{\varepsilon_{eq}}{6\alpha'}, 0 \right\} \tag{7}$$

where $R_{\varepsilon_{eq}}$ is defined as the relative dent severity based on the equivalent strain

3. Experimental program

3.1. Materials and specimen preparation

Laboratory experiments were carried out to evaluate the iterative effects of bending and dent that occurred at the same position of pipes. The material of investigated steel pipes is commonly used for the transmission lines of natural gas and hydraulic fluid according to standard ASTM A500 [50]. The outer diameter and the wall thickness of the pipes were 114.3 mm (4.5 in.) and 6.02 mm (0.237 in.), respectively, as

specified by the manufacturer. Two different lengths (1550 mm and 2550 mm) of pipes were tested. The chemical composition and mechanical properties of the investigated pipes are listed in Table 1.

Distributed fiber optic strain sensors were installed on the surface of pipe specimens in the designed layout according to following steps:

- Before the installation of sensors, the pipes were immersed in an acetic acid solution (concentration: 5%) to remove surface rust, and they were cleaned using alcohol wipes.
- Fiber optic cables for strain measurement were attached to the exterior surface of each pipe using tapes at discrete spots, following the designed helix pattern. The tape was used to temporarily hold fiber optic cables in place.
- A fast-setting ethyl cyanoacrylate glue (commonly known as "super glue" or "strain gauge glue"; manufacturer: Starbond; viscosity: 150 cPs) was used to attach the fiber optic cables to the pipes at discrete points between the tapes. Once the glue was set, the tapes were removed. The removal of tape must be careful to prevent damage to the fiber optic cables.
- A two-part epoxy (manufacturer: ProMarine Supplies) was applied to the fiber optic cables for a strong attachment with reliable strain transfer between the pipe and fiber optic cables. The epoxy was a mix of two components (i.e., resin and hardener) with a mixing ratio of 1:1 by volume. The thickness of epoxy was about 250 μm , which was around one tenth of the thickness of the pipes. The width of epoxy path was about 4 mm to 6 mm. Epoxy was cured in air at room temperature (22 °C \pm 2 °C) and under normal humidity (50% \pm 5%) for 24 h.

3.2. Test set-up, instrumentation, and loading protocol

Each pipe was loaded under four-point bending to generate bending and dent deformations at the middle span using a load frame, as shown in Fig. 5(a). The pipes were supported by two V-shaped blocks and vertically loaded by two rollers attached to a spreader beam at the middle span. The distance between two loading points was 750 mm. The distances between two supports were listed in Table 2.

The tests were conducted under displacement control at a constant

 Table 1

 Chemical composition and mechanical properties of investigated pipelines.

Chemical	С	Mn	P	S	Cu
compositions (wt%)	≤ 0.3	≤ 1.4	≤ 0.045	≤ 0.045	≥ 0.18
Mechanical properties	Elastic modulus <i>E</i> (GPa)	Yielding strength σ_{yd} (Mpa)	Tensile strength σ_t (Mpa)	Elongation (%)	σ_{yd}/σ_t
	≥ 200	≥ 290	≥ 400	≥ 23	≤ 0.9

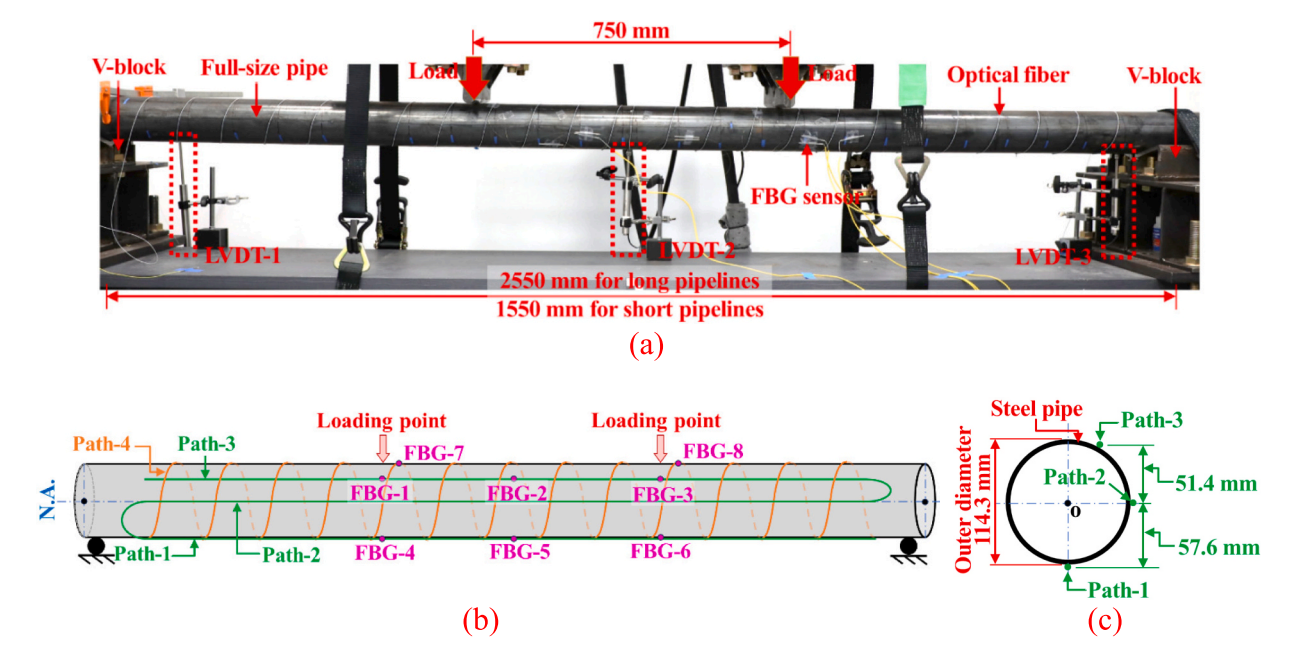


Fig. 5. Test set-up and sensor installation of a representative steel pipe subjected to four-point loading: (a) photograph of test set-up; (b) layout of sensor (in green and orange colors) installed on the pipe - elevation view; (c) layout of sensor installed on the pipe - cross section view. Dash lines indicate fiber optic cables deployed at the back side of the specimen. (For interpretation of the references to color in this figure legend, the reader is referred to the web version of this article.)

 Table 2

 Investigated cases for interactive effect of dent and bending deformation.

Category	Group	Sensor deployment pattern	Adjacent helix spacing (mm)	Distance between two supports (mm)
A	S1	Longitudinal (control)	-	1550 mm
	S2	Longitudinal (control)	-	1550 mm
	S3	Helix + Longitudinal	50	1550 mm
	S4	Helix + Longitudinal	50	1550 mm
	S5	Helix + Longitudinal	50	1550 mm
	S6	Helix + Longitudinal	100	1550 mm
В	S7	Helix + Longitudinal	100	2550 mm
	S8	Helix + Longitudinal	100	2550 mm

displacement rate (1 mm/min). The applied loads were measured by a load cell embedded in the load frame. Three linear variable differential transformers (LVDTs) were used to measure the displacements of two supports and the mid-span section of the pipes. A high-resolution camera was utilized to provide computer vision measurements of the deformations of pipes.

The deployment of the fiber optic cables is shown in Fig. 3 and Fig. 5. One end of the fiber optic cable was connected to the data acquisition system (model: Luna ODiSi 6102) to perform OFDR measurements, and the other end of the fiber optic cable was free. Path-1 to Path-3 (green color in Fig. 5(b)) were installed along the length direction of the pipe specimen firstly, and then Path-4 (orange color in Fig. 5(b)) was installed in a helix pattern along the circumference direction of the pipe specimen. Path-1 was installed at the bottom of the pipe; Path-2 was installed along the neutral axis of the pipe; Path-3 was installed near the top of the pipe, and the precise position of Path-3 is shown in Fig. 5(c). The distance between adjacent helix lines of Path-4 for each pipe

specimen is detailed in Table 2. In addition to the use of DFOS, eight fiber Bragg grating (FBG) sensors were installed on Path-1 to Path-4 along the same direction as the DFOS to provide an additional set of strain measurement data.

3.3. Investigated cases

A total of eight pipe specimens were investigated, which were grouped into two categories, designated as S1 to S6 for Category A and S7 to S8 for Category B. Specimens S1 to S6 were short pipelines with a 1550-mm distance between the two supports. Specimens S7 to S8 were long pipelines with a 2550-mm distance between the two supports.

Specimens S1 and S2 were the reference specimens, which were intact before the load testing. For specimens S3 to S8, the contact surfaces of sections under loading points were pre-weakened by pre-loading those section under loads up to 110 kN to generate local imperfections which then promoted the generation of local dents during the formal testing. Specimens S1 to S6 were used to investigate the interactive effect of bending and dent, the layout of fiber optic cables, and the distance between adjacent loops of fiber optic cables for short pipes. Specimen S7 and S8 were used to investigate the interactive effect of bending and dent for long pipes. The details of the sensor deployment and adjacent helix spacing of optical fiber are listed in Table 2.

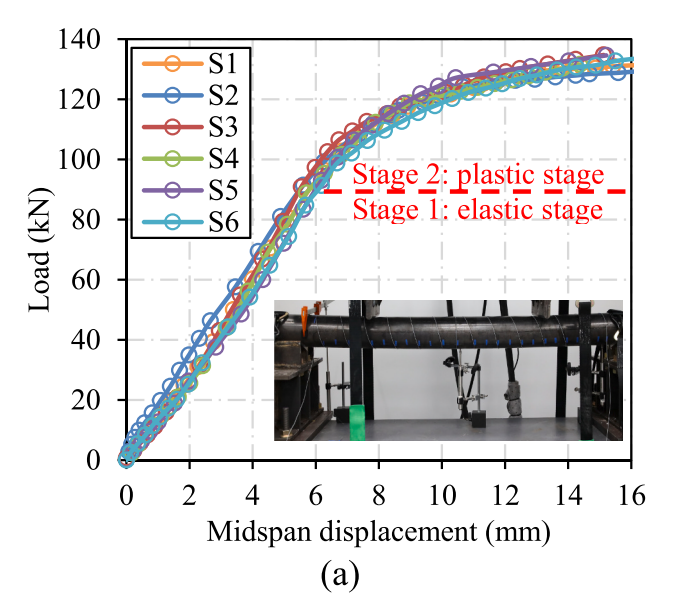
4. Results and discussions

4.1. Load-displacement curves

The load-displacement curves of the pipes are shown in Fig. 6. All pipes showed similar two-stage curves: (1) elastic stage, where the load linearly increases with the displacement; and (2) plastic stage, where the load increases with the displacement with a decreasing slope. The pipes exhibited typical global bending deformations and local dent deformations at the two loaded points.

4.2. Strain distributions

Representative strain distributions measured from DFOS are shown



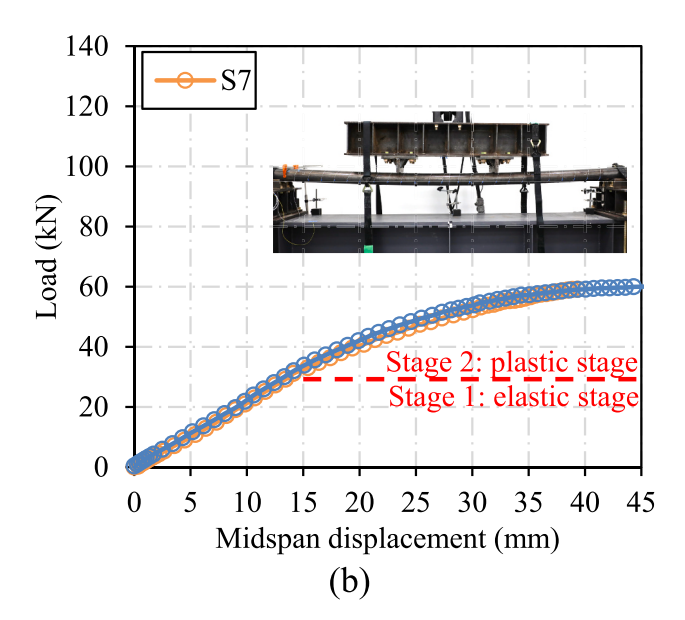


Fig. 6. Load-displacement curves of specimens under bending: (a) S1 to S6; and (b) S7 and S8.

in Fig. 7. The vertical axis represents the measured strain values, and the horizontal axis represents the distance along the length of DFOS, with the zero distance at the connector of the data acquisition system. In each figure, the length range of the DFOS has been selected to show the strain distributions within the length of fiber optic cables installed on the pipe specimen, and the length of fiber optic cable that is not attached to the pipe is not displayed. In each figure, the curves that are shown in different colors represent the strain distributions measured from DFOS deployed on pipes under different load levels. As the applied load increases, the magnitude of strain increases correspondingly. The lengths of the pipes that are subjected to interactive bending and dent are marked using green boxes. The strain distributions in each path are not perfectly symmetrical because the loads applied at the two loaded sections are slightly different due to the adopted test setup.

In specimen S5, the strain distributions on Path-1 at the bottom of the pipe showed typical global flexural strain distribution under four-point bending, and only two very small local peaks at the point loads were observed in the bottom strains, which indicates that the interactive effect is not obvious. However, for Path-2 at the neutral axis of the pipe and Path-3 near the top of the pipe, an obvious interactive effect was observed at the two loading points, which makes it easy to detect and locate the pipe length subjected to the interactive effect of bending and dent. The non-zero neutral axis strain distributions along the full length of Path-2 in Fig. 7(a), Fig. 7(c), and Fig. 7(e) are attributed for multiple reasons. The primary reasons for the non-zero neutral axis strains are due to localized circumferential deflections and stress concentration, as discussed in reference [51]. The secondary reasons include slight shift of the position of the fiber optic sensor in Path-2 from the neutral axis of the pipe in the sensor installation process, and slight rotation of pipe in the loading process. Regarding Path-4 in a helix pattern, the strain distributions near the two loading points showed an "M" shape, which is consistent with the interactive effect of bending and dent shown in Fig. 3. With distributed fiber optic sensor network of Path-1 to Path-4, the interactive region was determined along the longitudinal direction and helix direction. The results from different specimens are slightly different, but the trends are consistent overall.

The strains measured from distributed fiber optic sensors and FBG sensors were compared in Fig. 8. FBG-1 to FBG-6 measured strains along the longitudinal direction in Path-1 to Path-3; and FBG-7 and FBG-8 measured strains along the helix direction in Path-4. The data is analyzed via linear regression, and a coefficient of determination (\mathbb{R}^2) is calculated for each sensing point. The slope of the fitting line is used to

correct the results from the distributed sensors. The results indicate a strong correlation between the results obtained from the distributed and FBG sensors.

4.3. Deformed profiles

The bending deformations of the pipe specimens were reconstructed according to eq. (5) and compared with the data from the computer vision system and three LDVTs, as shown in Fig. 9(a). The solid lines represent the shapes of the deformed pipe obtained from computer vision [20], and the black dash lines represent the shapes of the deformed pipe derived from the strain distributions measured from DFOS [20]. Symbols "*" show the deflections of the pipe obtained from the three LVDTs. The considered load increased from 0 to 60 kN. Fig. 9 (b) indicates that the deformed shapes obtained from the three methods are consistent, highlighting the efficacy of the deformation reconstruction methods based on computer vision and DFOS.

Fig. 9(c) compares the strain reconstruction results and LVDT-2 measurement results of mid-span deflection of pipe bottom. The calculation and measurement results of mid-span deflections agree well with each other. A straight line can be used to fit the data, and the coefficient of determination (R^2) is 0.9999, which indicates a robust correlation. The slope of the fitting line (0.9967) is used to correct the results from the distributed sensors. The discrepancies among the deflections obtained from three methods were attributed to inherent inaccuracy of the sensors, data acquisition systems, and positions of the distributed sensor. For example, the fiber optic cables were not exactly installed at the bottom lines of pipes, and the pipes were rotated slightly in the loading process.

4.4. Strain-based dent severity evaluation

Strain distributions from Path 1 to Path 4 cover both length and circumference direction, and the intersection points of different paths can be used to evaluate the severity of dent deformation, as shown in Fig. 10(a). However, due to the inclined angle of Path 4 in a helix pattern, the strain distributions from Path-4 cannot be used for evaluation directly. The circumferential strains (ε_y) of intersection points is calculated according to eq. (8):

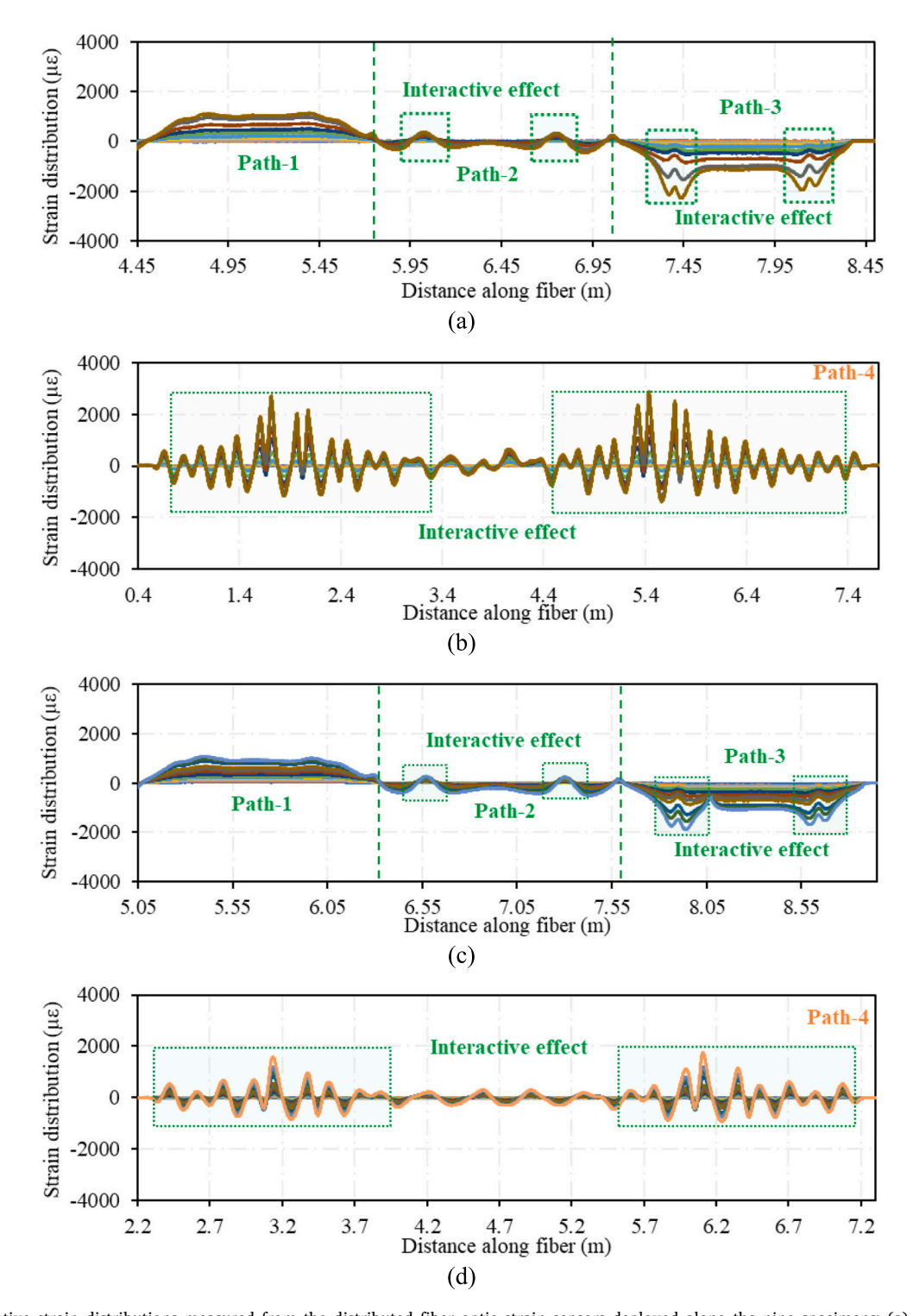


Fig. 7. Representative strain distributions measured from the distributed fiber optic strain sensors deployed along the pipe specimens: (a) Path-1 to Path-3 of specimen S5; (b) Path-4 of specimen S5; (c) Path-1 to Path-3 of specimen S6; (d) Path-4 of specimen S6; (e) Path-1 to Path-3 of specimen S8; and (f) Path-4 of specimen S8.

$$\varepsilon_{y} = \frac{\varepsilon_{f_{4}}}{\sqrt{1 + \alpha^{2}}} \tag{8a}$$

$$\alpha = \frac{s}{\pi (2R + t + r_f)} \tag{8b}$$

where ε_{f_4} is the strains obtained from fiber optic cable Path-4 (helix path); α is defined to consider the inclined angle between helix path and

pipe axis direction; s is the distance between adjacent helix path of Path-4; and r_f is the radius of outer coating of the fiber optic cable.

By substituting Eq. (8) into Eqs. (6) and (7), the severity of dent can be evaluated. The dent severity indicator ($R_{\epsilon_{eq}}$) at the intersection points can be further converted into engineer-friendly images to interpret the data for assessing dent. Representative results for pipe specimen S8 are shown in Fig. 10(b). The images are created by performing coordinate

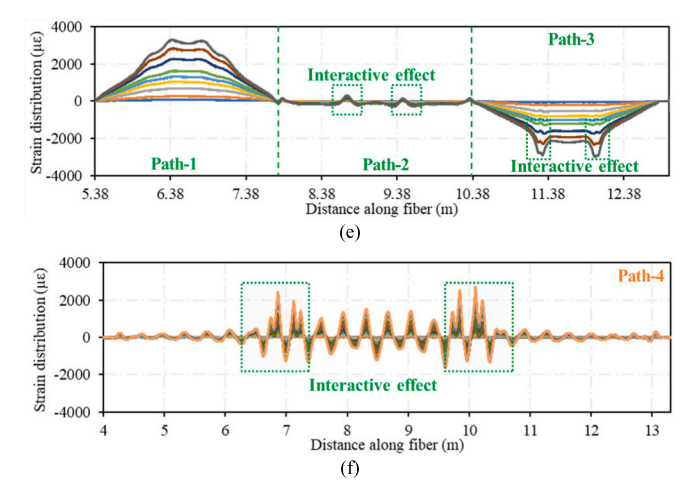


Fig. 7. (continued).

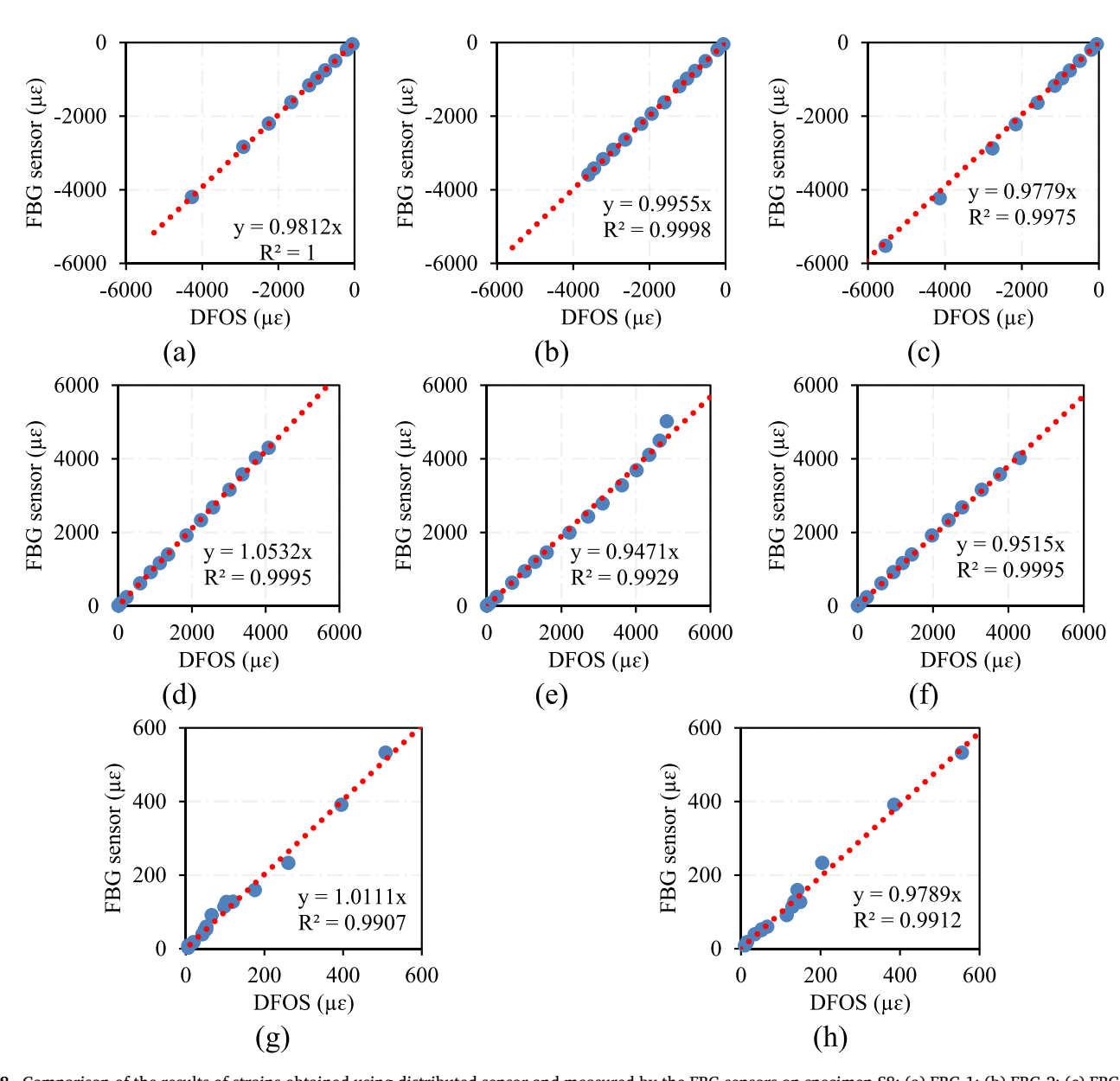


Fig. 8. Comparison of the results of strains obtained using distributed sensor and measured by the FBG sensors on specimen S8: (a) FBG-1; (b) FBG-2; (c) FBG-3; (d) FBG-4; (e) FBG-5; (f) FBG-6; (g) FBG-7; and (h) FBG-8.

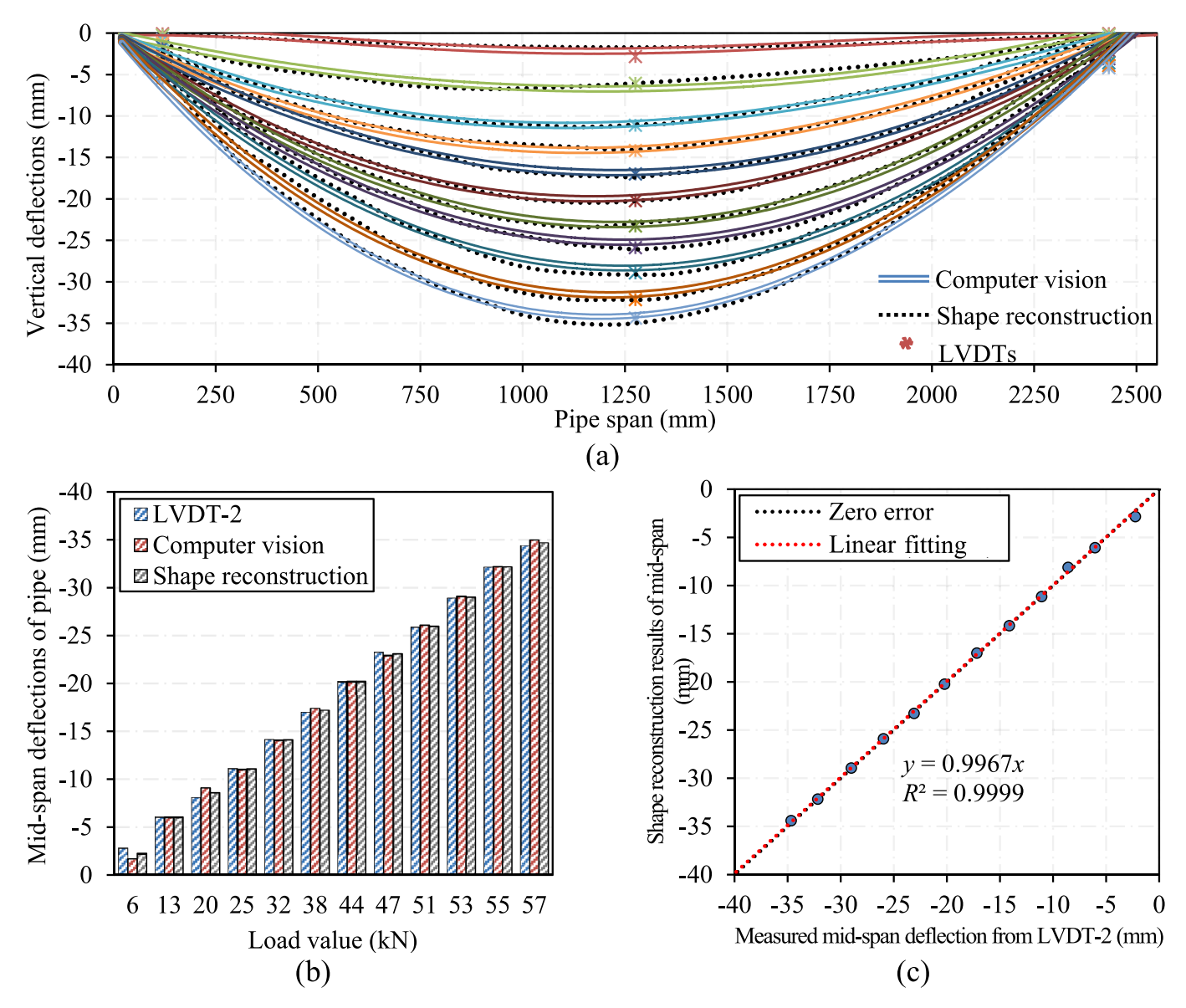


Fig. 9. Deformation results from of the bottom of specimen S8 obtained from shape reconstruction, LVDTs, and computer vision: (a) vertical deflection results; (b) comparison of mid-span deflections from three results; (c) measurement accuracy of the mid-span deflection of pipe bottom.

correlation: The round surface of the pipe is unfolded to a plane. Half circumference of the pipe is the height of the plane, and the length of the pipe is the length of the plane. The black dots on the plane show the intersection points.

By correlating the coordinates, the relative dent severity ($R_{\epsilon_{eq}}$) of the steel pipe can be mapped to a plane. Because Path 1 to Path 3 were installed on the front of pipes, only a half of the external surface is displayed, and the other half can be obtained by symmetry. The data between adjacent intersection points were obtained through biharmonic interpolation by using the surface fitting function of MATLAB [19]. Then, the full contours of relative dent severity under different loads were plotted to visualize dent severity.

In Fig. 10(b), the legend shows that the colors represent the magnitude of relative dent severity ($R_{\varepsilon_{eq}}$). The areas of the pipe subjected to high relative dent severity values are shown in red color, indicating that the areas have severe dent. It is observed that the local dent effect became obvious until the loading value was larger than 30 kN, which is consistent with the load-displacement curve. The locations and severity of the dent identified from the contours were also in good agreement with the visual inspection results.

4.5. Discrimination of dent and bending

The strain distributions on Path-4 were used to differentiate bending and dent deformations. With the increase of loads, strain distributions were turned into a frequency domain and replotted into a power spectrum, as shown in Fig. 11. The magnitude of power at the maximum load level is normalized to one and represented by color. It is observed that global bending effect occurred from the beginning of the test, but the local dent effect became obvious until the loading value was larger than 30 kN, which is consistent with the load-displacement curve.

Moreover, if the normalization strategy is changed to: The magnitudes of powers at each load level are normalized to one (Fig. 12), it is observed that local stress concentration effect is detected almost from the beginning of the test (the loading value was smaller than 8 kN), which is much earlier than the occurring of local dent effect. Such early detection capability of local stress concentration is promising to enhance the safety and operational management of pipelines.

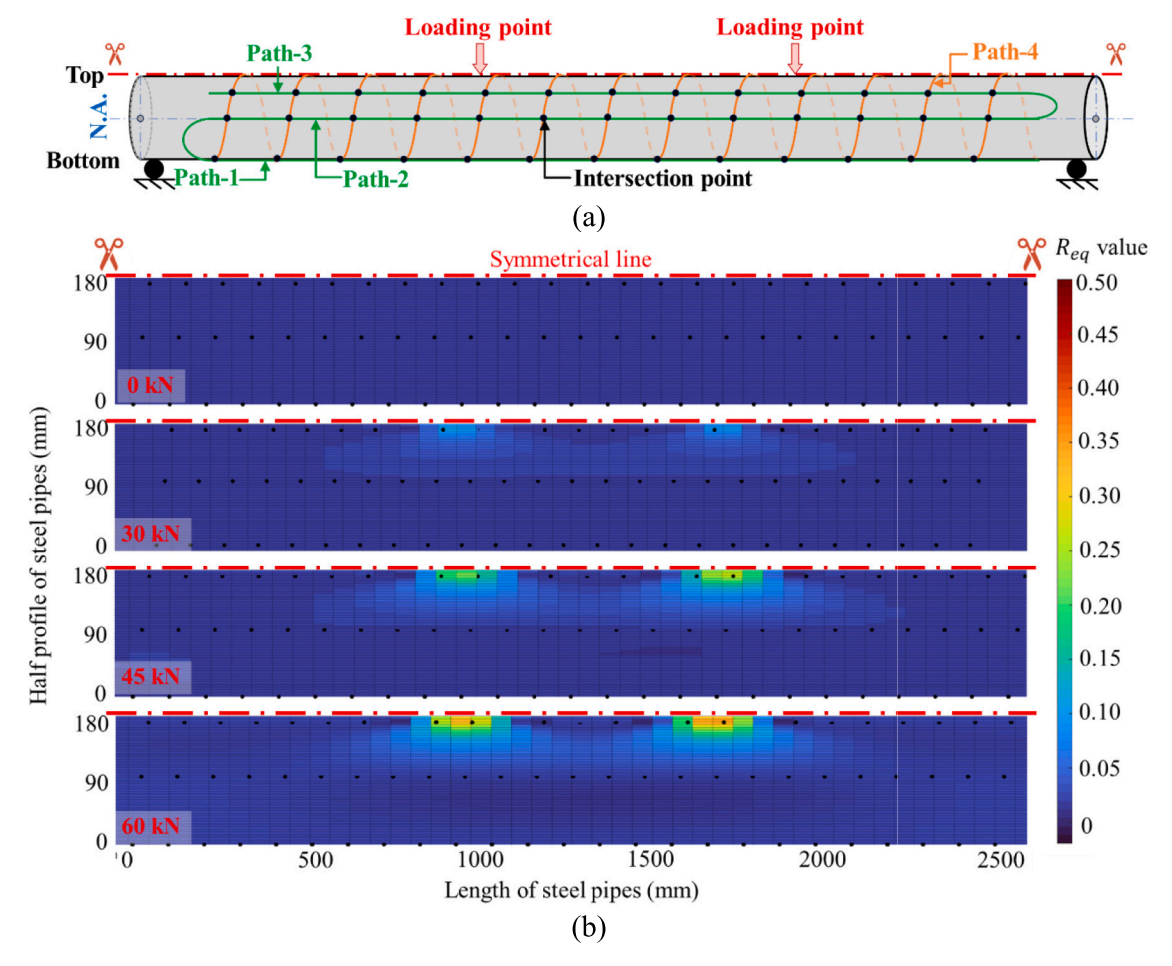


Fig. 10. Severity of dent deformation of pipe specimen S8: (a) distribution of intersection point on pipes for evaluating dent severity; and (b) development of dent severity under increasing loads.

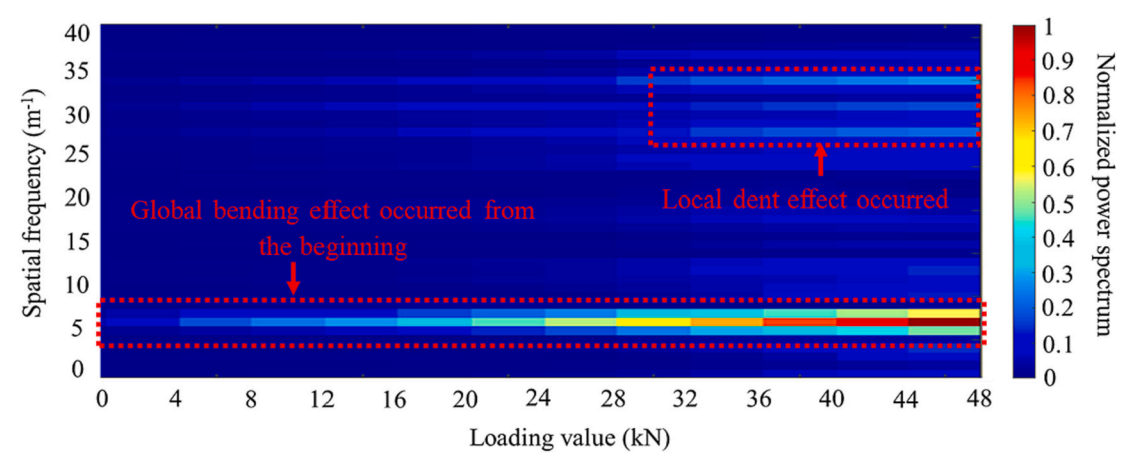


Fig. 11. Normalized power spectrum of a strain distribution for differentiating bending and dent.

4.6. Limitations and future research

This research represents a feasibility study on the monitoring of interactive effects of bending and dent in pipelines using distributed fiber optic sensors in a laboratory setting. Future research needs to be performed to further understand the performance in field applications. In real practices, many practical factors must be considered, such as the cost related to the sensor, the sensing range of a single fiber optic cable, the durability of the adhesive.

The cost includes the cost of fiber optic cables, sensor installation and maintenance cost, as well as sensor operation cost. One of the advantages of the presented sensing technology is that the fiber optic cable is a commercial telecommunication-grade single-mode fiber optic cable which is cost-effective compared with other types of sensors such as fiber Bragg grating sensors. The unit price of single-mode fiber optic cable is at a scale of 0.1 dollar per meter.

The fiber optic cable can be embedded in or attached to the surface of monitored structure using adhesives. In this study, the fiber optic cable

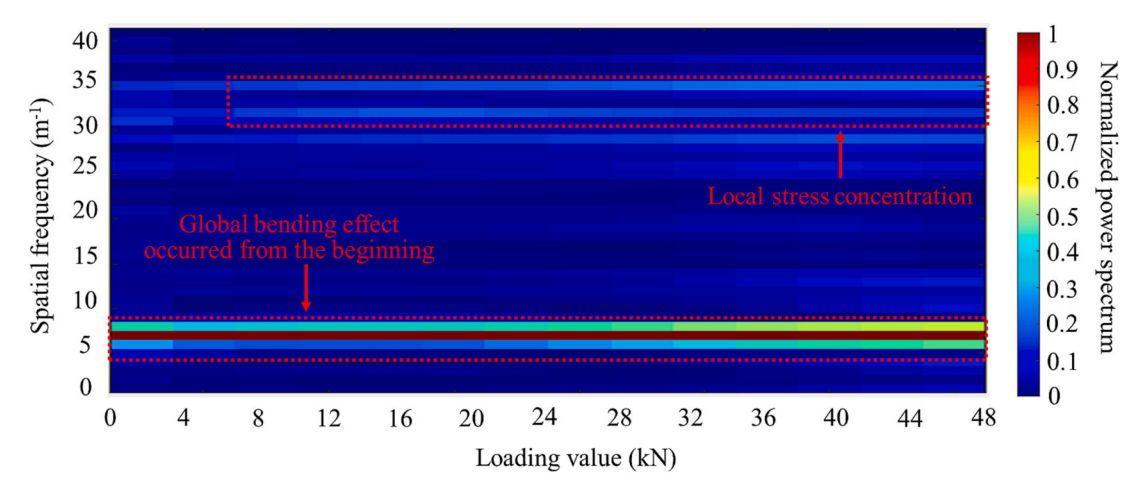


Fig. 12. Normalized power spectrum of a strain distribution for identifying stress concentration.

was manually installed with a speed of 5 m per minute roughly, and it is possible to automatically install fiber optic sensors using robots in the future. The lifespan of the distributed fiber optic sensor is mainly controlled by the lifespan of adhesives. In this study, a two-part epoxy was utilized as the adhesive. When epoxy is maintained well, the lifespan can be 20 years or longer. If a longer lifespan is needed, more durable adhesives such as ceramic adhesive which can bear with harsh environment can be adopted to replace epoxy in the installation of fiber optic cables.

The sensor operation cost mainly includes the costs related to the data acquisition system and operator. Although the data acquisition system involves an upfront cost, a system can be shared to operate many fiber optic sensors simultaneously. For example, the distributed fiber optic sensing system used in this research has eight channels, and the measurement length of each channel is longer than 200 m. When the sensor gauge length is set at 0.65 mm, each channel provides >300 measurement points in each measurement, and the eight channels provide >2400 measurement points, equivalent to >2400 individual point sensors. In this research, the distributed fiber optic sensor data were analyzed manually using the proposed approach; however, it is possible to perform data analysis and interpretation using machine learning models because various machine learning methods have been developed to automatically interpret distributed fiber optic sensor data for monitoring cracks [52,53].

In real practice, pipelines are subjected to more complex effects such as corrosion and cracks, which may also compromise the durability of the epoxy glue and optical fibers. For instance, fiber optic cables can possibly be cut by severe dents and cracks. It is essential to further develop the monitoring technologies by considering more types of interactive anomalies and long-term interactive effects in future research. A threshold-based warning method needs to be developed

based on assessment data for real-time alarm of pipeline condition.

The discrimination of bending and dent effects relies on relatively simple data analysis in this research, aiming to develop an engineer-friendly data analysis protocol. However, the powers of the bending and dent effects are largely unbalanced, and the bending effect has a higher power than the dents, as shown in Fig. 11 and Fig. 12, making it inconvenient to identify dents precisely. It is promising to develop more advanced data processing and analysis methods based on signal analysis and machine learning to achieve intelligent interpretation of the DFOS data [52–54].

To digitalize pipelines for automation in maintenance and management, Fig. 13 is presented based on the monitoring methods developed in this research. The function of DFOS that provides real-time monitoring of the pipeline condition is similar to the function of "sensory nerves" that sense the condition of biological systems. This paper has addressed the measurement of detailed strain distributions and interpretation of DFOS data. Further research is needed for developing the digital model of pipeline which is updateable by using the DFOS data in real time. The digital model can be accessed in mobile devices, as stated in reference [27].

5. Conclusions

This paper presents an approach to assess and discriminate interactive bending and dent in pipelines using DFOS, aiming at enhancing the ability to monitor the interactive anomalies of pipelines. Based on the above investigations, the following conclusions are drawn:

 Distributed fiber optic sensors can be used to monitor interactive bending and dent via measuring the detailed strain distributions of pipelines subjected to mechanical loads. The measured strain

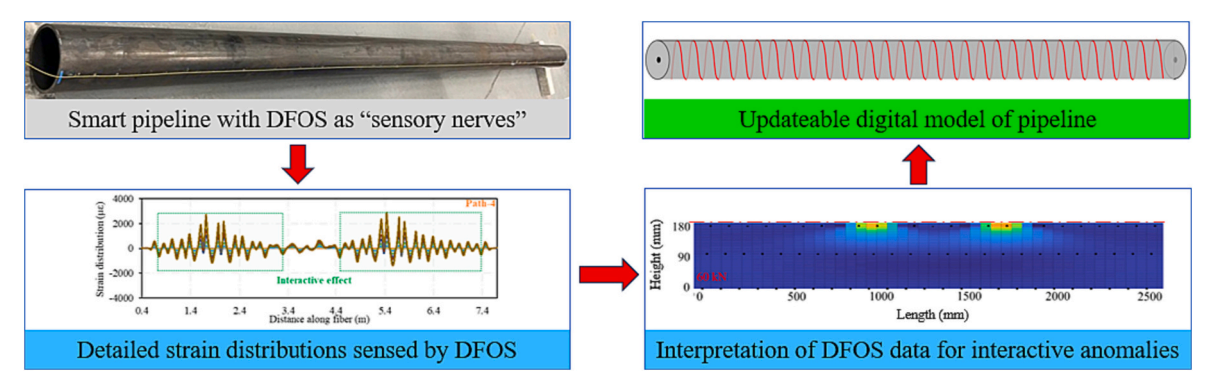


Fig. 13. Flowchart of achieving updateable digital models of pipelines by utilizing DFOS data.

- distributions can be utilized to trace, localize, and discriminate the interactive effect of bending and dent, which represent global and local deformations.
- The interactive effect of bending and dent can be monitored using the proposed normalized three-dimensional power spectrum method. The initiation and development of stress concentration can be located and assessed from an early state (load <8 kN), much earlier than the occurring of dent (load >30 kN). Such an early detection capability is important for enhancing the safety of pipelines.
- The proposed methods for evaluating deformed shapes achieved high accuracy ($R^2 = 0.9999$). The evaluation results of the bending deformations of the pipe specimens were validated using the evaluation results from computer vision and LVDTs. The locations and the severity of local dent deformations of the pipe specimens identified from the contours were consistent with the load-displacement curves and the visual inspection results at different load levels.

CRediT authorship contribution statement

Xiao Tan: Writing – original draft, Visualization, Validation, Software, Investigation, Formal analysis, Data curation. Sina Poorghasem: Writing – review & editing, Validation, Software, Investigation, Data curation. Ying Huang: Writing – review & editing, Validation, Software, Resources, Methodology, Investigation. Xin Feng: Writing – review & editing, Validation. Yi Bao: Writing – review & editing, Visualization, Supervision, Resources, Project administration, Methodology, Funding acquisition, Conceptualization.

Declaration of competing interest

The authors declare the following financial interests/personal relationships which may be considered as potential competing interests:

Yi Bao received funding from United States Department of Transportation and United States National Science Foundation.

Data availability

Data will be made available on request.

Acknowledgement

This research was funded by the PHMSA of United States Department of Transportation [grant numbers 693JK31950008CAAP and 693JK32310008POTA] and United States National Science Foundation [grant number CPS 2305882]. The authors acknowledge the discussion with Mr. Soroush Mahjoubi from Stevens Institute of Technology for the modification of Fig. 12.

References

- L. Zou, X. Bao, F. Ravet, L. Chen, Distributed Brillouin fiber sensor for detecting pipeline buckling in an energy pipe under internal pressure, Appl. Opt. 45 (14) (2006) 3372–3377, https://doi.org/10.1364/AO.45.003372.
- [2] ASTM-G96-90, Standard guide for online monitoring of corrosion in plant equipment (electrical and electrochemical methods), ASTM Int. (2018), https://doi.org/10.1520/G0096-90R18.
- [3] Michael Baker Jr., Inc, TTO Number 10, Integrity Management Program Delivery Order DTRS56-02-D-70036: Dent Study - Final Report, Office of Pipeline Safety, Research and Special Programs Administration, U.S. Department of Transportation, 2004. https://www.phmsa.dot.gov/sites/phmsa.dot.gov/files/docs/technical-res ources/pipeline/gas-transmission-integrity-management/65291/tto10dentstudyfi nalreportnov2004.pdf. Accessed on January 5, 2023.
- [4] J. Tikka, R. Hedman, A. Silijander, Strain gauge capabilities in crack detection, in: 4th International Workshop on Structural Health Monitoring, 2003, pp. 15–17. htt ps://publications.vtt.fi/julkaisut/muut/2003/iwshm2003_crackdetection.pdf. Accessed on September 12, 2023.
- [5] E. Muñoz, M.J. Rosenfeld, U.S. DOT/PHMSA DTPH56-14-H-00004: improving models to consider complex loadings, operational considerations, and interactive

- threats, Kiefner and Associates, 2016. https://primis.phmsa.dot.gov/matrix/FilGet.rdm?fil=11059 (Accessed on November 20, 2023).
- [6] I.B. Iflefel, D.G. Moffat, J. Mistry, The interaction of pressure and bending on a dented pipe, Int. J. Press. Vessel. Pip. 82 (2005) 761–769, https://doi.org/ 10.1016/j.ijpvp.2005.06.002.
- [7] P. Guo, W. Meng, Y. Bao, Automatic identification and quantification of dense microcracks in high-performance fiber-reinforced cementitious composites through deep learning-based computer vision, Cem. Concr. Res. 148 (2021) 106532, https://doi.org/10.1016/j.cemconres.2021.106532.
- [8] T. Wells, R.E. Melchers, An observation-based model for corrosion of concrete sewers under aggressive conditions, Cem. Concr. Res. 61 (2014) 1–10, https://doi. org/10.1016/j.cemconres.2014.03.013.
- [9] M.E. Haertel, J.R. Melo, M. Reck, D. Becker, J.M. Santos, C.S. Camerini, Development of an optical system for geometric inspection of external surface of pipelines, in: Optics and Photonics for Information Processing vol. VI, 8498, International Society for Optics and Photonics, 2012, p. 84980M, https://doi.org/ 10.1117/12.930268.
- [10] J. Valença, E. Júlio, H.J. Araújo, Applications of photogrammetry to structural assessment, Exp. Tech. 36 (5) (2012) 71–81, https://doi.org/10.1111/j.1747-1567.2011.00731.x.
- [11] S.W. Choi, B.R. Kim, H.M. Lee, Y. Kim, H.S. Park, A deformed shape monitoring model for building structures based on a 2D laser scanner, Sensors 13 (5) (2013) 6746–6758, https://doi.org/10.3390/s130506746.
- [12] J.F. Destrebecq, E. Toussaint, E. Ferrier, Analysis of cracks and deformations in a full scale reinforced concrete beam using a digital image correlation technique, Exp. Mech. 51 (6) (2011) 879–890, https://doi.org/10.1007/s11340-010-9384-9.
- [13] N. Gloria, M. Areiza, I. Miranda, J. Rebello, Development of a magnetic sensor for detection and sizing of internal pipeline corrosion defects, NDT E Int. 42 (8) (2009) 669–677, https://doi.org/10.1016/j.ndteint.2009.06.009.
- [14] H. Lei, Z. Huang, W. Liang, Y. Mao, P. Que, Ultrasonic pig for submarine oil pipeline corrosion inspection, Russ. J. Nondestruct. Test. 45 (4) (2009) 285–291, https://doi.org/10.1134/S106183090904010X.
- [15] M. Gao, R. Krishnamurthy, Mechanical damage in pipelines: A review of the methods and improvements in characterization, evaluation, and mitigation, Oil Gas Pipel. (2015) 289–326, https://doi.org/10.1002/9781119019213.ch22.
- [16] P.D. Panetta, A.A. Diaz, R.A. Pappas, T.T. Taylor, R.B. Francini, K.I. Johnson, Mechanical damage characterization in pipelines, Pacific Northwest National Laboratory, United States Department of Energy, Richland, WA, 2001. https://citeserx.ist.psu.edu/document?repid=rep1&type=pdf&doi=af9f1e124e2563c1b39a9 0f9a8088820a44f777 (Accessed on November 5, 2022).
- [17] Y. Liu, Y. Bao, Review on automated condition assessment of pipelines with machine learning, Adv. Eng. Inform. 53 (2022) 101687, https://doi.org/10.1016/j. aei 2022 101687
- [18] M. Gao, R. Krishnamurthy, R. McNealy, NO. PR-328-063502: investigate fundamentals and performance improvements of current in-line-inspection technologies for mechanical damage detection, phase II report, Blade Energy Partners (2009) 6–54. https://primis.phmsa.dot.gov/matrix/FilGet.rdm?fil=5074 (Accessed on November 5, 2022).
- [19] R. Schmidt, Unpiggable pipelines—What a challenge for in-line inspection!, Pigging Products and Services Association (PPSA), 2004. https://ppsa-online.com/paper s/2004-Aberdeen-7-Schmidt.pdf. Accessed on November 5, 2022.
- [20] X. Tan, P. Guo, X. Zou, Y. Bao, Buckling detection and shape reconstruction using strain distributions measured from a distributed fiber optic sensor, Measurement 200 (2022) 111625, https://doi.org/10.1016/j.measurement.2022.111625.
- [21] Y. Bao, M. Valipour, W. Meng, K.H. Khayat, G. Chen, Distributed fiber optic sensor-enhanced detection and prediction of shrinkage-induced delamination of ultra-high-performance concrete overlay, Smart Mater. Struct. 26 (8) (2017) 085009, https://doi.org/10.1088/1361-665X/aa71f4.
- [22] M. Yan, X. Tan, S. Mahjoubi, Y. Bao, Strain transfer effect on measurements with distributed fiber optic sensors, Autom. Constr. 139 (2022) 104262, https://doi. org/10.1016/j.autcon.2022.104262.
- [23] P. Lu, R.F. Wright, M. Ziomek-Moroz, M.P. Buric, P. Zandhuis, P.R. Ohodnicki, A multifunctional fiber optic sensor for internal corrosion monitoring in natural gas transmission pipelines, in: NACE International Corrosion Conference Proceedings, 2018, pp. 1–12. https://search.proquest.com/docview/2463181656/fulltext PDF/CF8E54A96DAD46C1PQ/1?accountid=14052. Accessed on November 5, 2023
- [24] X. Feng, Y. Han, Z. Wang, H. Liu, Structural performance monitoring of buried pipelines using distributed fiber optic sensors, J. Civ. Struct. Heal. Monit. 8 (3) (2018) 509–516, https://doi.org/10.1007/s13349-018-0286-3.
- [25] X. Tan, L. Fan, Y. Huang, Y. Bao, Detection, visualization, quantification, and warning of pipe corrosion using distributed fiber optic sensors, Autom. Constr. 132 (2021) 103953, https://doi.org/10.1016/j.autcon.2021.103953.
- [26] L. Ren, T. Jiang, D.S. Li, P. Zhang, H.N. Li, G.B. Song, A method of pipeline corrosion detection based on hoop-strain monitoring technology, Struct. Control. Health Monit. 24 (6) (2017) e1931, https://doi.org/10.1002/stc.1931.
- [27] M. Li, X. Feng, Y. Han, Brillouin fiber optic sensors and mobile augmented reality-based digital twins for quantitative safety assessment of underground pipelines, Autom. Constr. 144 (2022) 104617, https://doi.org/10.1016/j. autcon.2022.104617.
- [28] D. Inaudi, B. Glisic, Long-range pipeline monitoring by distributed fiber optic sensing, J. Press. Vessel. Technol. 132 (1) (2010) 011701, https://doi.org/ 10.1115/1.3062942.
- [29] R.F. Wright, M. Badar, J.C. Egbu, P. Lu, M. Buric, P.R. Ohodnicki Jr., Fully distributed optical fiber sensor for water and humidity monitoring, in: Fiber Optic

- Sensors and Applications XVI 11000, International Society for Optics and Photonics, 2019, p. 1100007, https://doi.org/10.1117/12.2519239.
- [30] X. Tan, Y. Bao, Q. Zhang, H. Nassif, G. Chen, Strain transfer effect in distributed fiber optic sensors under an arbitrary field, Autom. Constr. 124 (2021) 103597, https://doi.org/10.1016/j.autcon.2021.103597.
- [31] Y. Zhu, G. Chen, Heat treatment and polymer coating effect on Rayleigh scattering based fiber optic temperature measurement, Measurement 206 (2023) 112253, https://doi.org/10.1016/j.measurement.2022.112253.
- [32] L. Fan, X. Tan, Q. Zhang, W. Meng, G. Chen, Y. Bao, Monitoring corrosion of steel bars in reinforced concrete based on helix strains measured from a distributed fiber optic sensor, Eng. Struct. 204 (2020) 110039, https://doi.org/10.1016/j. engstruct.2019.110039.
- [33] S. Zhang, B. Liu, J. He, Pipeline deformation monitoring using distributed fiber optical sensor, Measurement 133 (2019) 208–213, https://doi.org/10.1016/j. measurement.2018.10.021.
- [34] W. Shen, Q. Pang, L. Fan, P. Li, X. Zhao, Monitoring and quantification of non-uniform corrosion induced mass loss of steel piles with distributed optical fiber sensors, Autom. Constr. 148 (2023) 104769, https://doi.org/10.1016/j.autcop.2023.104769
- [35] S. Rizzolo, J. Périsse, A. Boukenter, Y. Ouerdane, E. Marin, J.R. Macé, M. Cannas, S. Girard, Real time monitoring of water level and temperature in storage fuel pools through optical fibre sensors, Sci. Rep. 7 (1) (2017) 8766, https://doi.org/ 10.1038/s41598-017-08853-7.
- [36] N. Lalam, P. Westbrook, K. Naeem, P. Lu, P. Ohodnicki, N. Diemler, M.P. Buric, R. Wright, Pilot-scale testing of natural gas pipeline monitoring based on phase-OTDR and enhanced scatter optical fiber cable, Sci. Report. 13 (2023) 14037, https://doi.org/10.1038/s41598-023-41338-4.
- [37] H. Li, H. Zhu, D. Tan, B. Shi, J. Yin, Detecting pipeline leakage using active distributed temperature sensing: theoretical modeling and experimental verification, Tunn. Undergr. Space Technol. 135 (2023) 105065, https://doi.org/ 10.1016/j.tust.2023.105065.
- [38] H. Li, H. Zhu, H. Wu, B. Zhu, B. Shi, Experimental investigation on pipe-soil interaction due to ground subsidence via high-resolution fiber optic sensing, Tunn. Undergr. Space Technol. 127 (2022) 104586, https://doi.org/10.1016/j. https://doi.org/10.1016/j.
- [39] H. Lan, G. Ma, N.A. Hoult, I.D. Moore, Stress concentrations due to simulated corrosion pits in buried metal pipes under longitudinal bending, J. Civ. Struct. Heal. Monit. 12 (4) (2022) 785–796, https://doi.org/10.1007/s13349-021-00522-8
- [40] Luna ODiSI 6000 Data Sheet. https://lunainc.com/sites/default/files/assets/files/data-sheet/Luna%20ODiSI%206000%20Data%20Sheet.pdf, 2023. Accessed on June 1, 2023.
- [41] X. Tan, Y. Bao, Measuring crack width using a distributed fiber optic sensor based on optical frequency domain reflectometry, Measurement 172 (2021) 108945, https://doi.org/10.1016/j.measurement.2020.108945.

- [42] X. Tan, A. Abu-Obeidah, Y. Bao, H. Nassif, W. Nasreddine, Measurement and visualization of strains and cracks in CFRP post-tensioned fiber reinforced concrete beams using distributed fiber optic sensors, Autom. Constr. 124 (2021) 103604, https://doi.org/10.1016/j.autcon.2021.103604.
- [43] Y. Bao, W. Meng, Y. Chen, G. Chen, K.H. Khayat, Measuring mortar shrinkage and cracking by pulse pre-pump Brillouin optical time domain analysis with a single optical fiber, Mater. Lett. 145 (2015) 344–346, https://doi.org/10.1016/j. matlet.2015.01.140.
- [44] Y. Bao, G. Chen, Strain distribution and crack detection in thin unbonded concrete pavement overlays with fully distributed fiber optic sensors, Opt. Eng. 55 (1) (2015) 011008, https://doi.org/10.1117/1.0E.55.1.011008.
- [45] Y. Bao, F. Tang, Y. Chen, W. Meng, Y. Huang, G. Chen, Concrete pavement monitoring with PPP-BOTDA distributed strain and crack sensors, Smart Struct. Syst. 18 (3) (2016) 405–423, https://doi.org/10.12989/sss.2016.18.3.405.
- [46] Y. Bao, M.S. Hoehler, C.M. Smith, M. Bundy, G. Chen, Measuring threedimensional temperature distributions in steel–concrete composite slabs subjected to fire using distributed fiber optic sensors, Sensors 20 (19) (2020) 5518, https:// doi.org/10.3390/s20195518.
- [47] M. Ramezani, T. Neitzert, Strain based evaluation of dents in pressurized pipes, Int. J. Mech. Aerosp. Industr. Mech. Manufact. Eng. 7 (6) (2013) 974–979. https://citeseerx.ist.psu.edu/document?repid=re-p1&type=pdf&doi=8cd177d8689 157dae7facb08954243ce0f018a49 (Accessed on July 15, 2023).
- [48] J. Zhao, Y.R. Lv, Y.F. Cheng, Standards and methods for dent assessment and failure prediction of pipelines: A critical review, Pet. Sci. 19 (6) (2022) 3029–3045, https://doi.org/10.1016/j.petsci.2022.10.003.
- [49] A.N.M. Rafi, Structural behaviour of dented pipelines, Ph.D. Thesis, University of Windsor, 2011, https://scholar.uwindsor.ca/etd/89. Accessed on November 2, 2023
- [50] ASTM A500-03a, Standard specification for cold-formed welded and seamless carbon steel structural tubing in rounds and shapes, ASTM Int. (2017), https://doi. org/10.1520/A0500-03A.
- [51] J.A. Simmons, N.A. Hoult, I.D. Moore, Behavior assessment of exhumed cast Iron pipes using distributed strain sensing, J. Pipel. Syst. Eng. Pract. 15 (1) (2024) 04023051, https://doi.org/10.1061/JPSEA2.PSENG-14.
- [52] Y. Liu, Y. Bao, Intelligent monitoring of spatially-distributed cracks using distributed fiber optic sensors assisted by deep learning, Measurement 220 (2023) 113418, https://doi.org/10.1016/j.measurement.2023.113418.
- [53] Y. Liu, Y. Bao, Automatic interpretation of strain distributions measured from distributed fiber optic sensors for crack monitoring, Measurement 211 (2023) 112629, https://doi.org/10.1016/j.measurement.2023.112629.
- [54] A. Venketeswaran, N. Lalam, J. Wuenschell, P.R. Ohodnicki Jr., M. Badar, K. P. Chen, P. Lu, Y. Duan, B. Chorpening, M. Buric, Recent advances in machine learning for fiber optic sensor applications, Adv. Intell. Syst. 4 (1) (2022) 2100067, https://doi.org/10.1002/aisy.202100067.